Earth Planets Space, **63**, 351–357, 2011

Local empirical model of ionospheric plasma density derived from Digisonde measurements at Irkutsk

K. G. Ratovsky and A. V. Oinats

Institute of Solar-Terrestrial Physics, 664033, Lermontov st., 126a, P.O. Box 291, Irkutsk, Russia

(Received June 7, 2010; Revised March 7, 2011; Accepted March 7, 2011; Online published June 14, 2011)

Ionogram data from routine ionospheric observations in Irkutsk, Russia using a DPS-4 Digisonde sounder were hand-scaled for the 6-year period from December 2002 to December 2008 to derive a local empirical model of the electron density distribution in the bottomside ionosphere that provides a comprehensive description of the diurnal, seasonal, and solar activity variations of the major ionospheric characteristics. The paper describes the technique for building the local empirical model and the results of comparing its diurnal, seasonal, and solar activity specifications with the standard IRI-2007 climatological model for the same period of time, and retrospective observational data from the Millstone Hill incoherent scatter radar (1976–2002) and a collocated Digisonde (1989–1990, 1998–2004). Reasoning for the observed differences between the three datasets is then provided in terms of background physical phenomena. Primary focus of the paper is the behavior of three F_2 layer characteristics: the F_2 peak density (N_mF_2), the peak height (h_mF_2) and the bottomside thickness (B_0).
Key words: Local model, Digisonde, IRI model, diurnal-seasonal-solar activity behavior.

1. Introduction

The DPS-4 Digisonde (Reinisch *et al*., 1997) was installed at Irkutsk, Russia (52.3N, 104.3E) in November, 2002. All Digisonde ionogram data have been manually scaled using an interactive ionogram scaling software, SAO Explorer (Reinisch *et al*., 2004; Khmyrov *et al*., 2008). The electron density profiles (EDP) were inverted from all suitable ionogram traces using the NHPC method (Reinisch and Huang, 1983). In addition to the EDP itself, NHPC provides two standard IRI parameters for the EDP representation, the bottomside thickness B_0 and the shape parameter B_1 using the Reinisch and Huang (1998) technique. In order to validate the quality of the observational data, the ionospheric F region parameters measured with the DPS-4 were compared to available data from a co-located chirp-ionosonde (Brynko *et al*., 1988) and the Irkutsk incoherent scatter radar (Shpynev, 2004); this comparison revealed no systematic discrepancies between the data from the different instruments for quiet geomagnetic conditions (Ratovsky *et al*., 2005).

Six years of the hand-scaled ionospheric characteristics from December 2002 to December 2008 were used to build a local empirical model of ionospheric electron density (LEMI) for Irkutsk. The Irkutsk LEMI model complements monthly-median climatological ionospheric specifications provided by global models like the IRI-2007 (Bilitza and Reinisch, 2008) by accounting for the regional specifics of the ionospheric plasma distribution that elude detailed reproduction in a global model. Study of the comprehensive patterns of the diurnal, seasonal, and solar activity variations of ionospheric characteristics provided by LEMI makes our model a useful tool for understanding the physical mechanisms of these variations.

The following sections compare the LEMI diurnal, seasonal, and solar activity behavior with the IRI-2007 (Bilitza and Reinisch, 2008) prediction and with long-term observational data from the Millstone Hill (42.6N, 288.5E) incoherent scatter radar (1976–2002), the co-located ionosonde (1989–1990, 1998–2004) (Lei *et al*., 2004, 2005), and other instruments. Comparison of LEMI with data from a different mid-latitude location allowed us to identify the longitudinal differences in the local ionospheric specifications. We then discuss observed differences in the context of background physical phenomena. For the purpose of such comparison, we selected three F_2 layer parameters: the F_2 peak density (N_mF_2), the peak height (h_mF_2), and the bottomside thickness (B_0) and used the latest IRI-2007 model version (Bilitza and Reinisch, 2008) with the following options: URSI maps for N_mF_2, CCIR maps for h_mF_2, and the Gulyaeva option for B_0.

2. LEMI Construction Technique

The source data for the empirical model representation are the ionospheric characteristics obtained by the Irkutsk Digisonde operating at a 15-minute cadence. Each measured characteristic P is considered as a function of local time (LT), day of year (D) and year (Y), i.e., P (LT, D, Y). In order to represent the regular part of the observed P (LT, D, Y) behavior that we expect to be associated with climatological specifics of the diurnal, seasonal, and long-term solar activity variations, we used the 27-day sliding window median P_{med} (LT, D, Y) for each combination of LT, D, and Y in the sets $\{P$ (LT, D$-$13, Y), $\cdots$, P (LT, D+13,

doi:10.5047/eps.2011.03.002

Y}. As shown in numerous data analysis applications, use of the median filtering instead of a classic averaging preserves strong gradients in the source data while suppressing the short-term variability with periods below the filter length (27 days in our case). No data (including high magnetic activity conditions) were removed from the median calculations.

As a unit of annual variations we selected the month (M) equal to $T/12$, where $T = 365.25$ days is the solar year (Y_S). The solar year Y_S starts from the winter solstice of leap year (December 21). The month continuously varies from 0 to 12, the month = 0 corresponds to the beginning of Y_S. Since the same days of different years do not correspond exactly to equal month values, we transformed P_{med} (LT, D, Y) to P_{med} (LT, M, Y_S) at equal month steps using simple linear interpolation. Hereinafter, we use traditional month names, implying that the zero month is December, the 1st month is January, the 2nd is February, and so on. The beginnings of December and June correspond to the winter and summer solstices and the beginnings of March and September refer to the spring and autumn equinoxes.

Calculated P_{med} (LT, D, Y) are then converted into a P_{med} (LT, M, Y_S) representation suitable for describing the annual variations, where Y_S is the solar year, and the month M is equal to $T/12$, where $T = 365.25$ days of Y_S. The solar year Y_S starts from the winter solstice of a leap year (December 21). The month continuously varies from 0 to 12, with the 0th month corresponding to the beginning of Y_S. Since the same days of different years do not correspond exactly to equal month values, we had to transform P_{med} (LT, D, Y) to P_{med} (LT, M, Y_S) at equal one-month steps using a simple linear interpolation. In the rest of our manuscript, we use conventional month names, implying that the 0th month is December, the 1st month is January, etc. In this presentation, December begins on the winter solstice, June begins on the summer solstice, and March and September begin on the spring and autumn equinoxes.

The 27-day running medians were used as an input for LEMI. The main assumption is that the P_{med} (LT, M, Y_S) can be approximated by a linear function of a suitable solar activity index. As a solar activity proxy we selected the 10.7 cm solar radio flux ($F_{10.7}$) whose daily values are available from WDC-A in Boulder, Colorado (ftp://ftp.ngdc.noaa.gov/STP/SOLAR_DATA) in solar flux units s.f.u. (1 s.f.u. = 10^{-22} W m^{-2} Hz^{-1}). Dependence of P_{med} on Y_s is therefore replaced by a linear function on $F_{10.7}$, so that P_{med} (LT, M, $F_{10.7}$) is used for further derivations, with the source values of $F_{10.7}$ linearly interpolated to appropriately obtain the solar radio flux values for any given M and Y_S. Under assumption of its linear dependence on $F_{10.7}$, each model characteristic can be presented in the slope-intercept form:

$$P_{med}(\mathrm{LT, M}, F_{10.7}) = P_0(\mathrm{LT, M}) + P_D(\mathrm{LT, M}) \cdot (F_{10.7} - F_{10.70})/F_{10.7100}, \quad (1)$$

where P_0 is the intercept value of the characteristic P_{med} for the low solar activity of $F_{10.70} = 70$ s.f.u. and P_D is the slope value, $dP_{med}/dF_{10.7}$, describing how sensitive the characteristic P is to changes in the solar activity. For convenience of the presentation the P_D values are calculated per increment of $F_{10.7100} = 100$ s.f.u., and in the remainder of this manuscript they are expressed in the units of (characteristic unit / 100 s.f.u.).

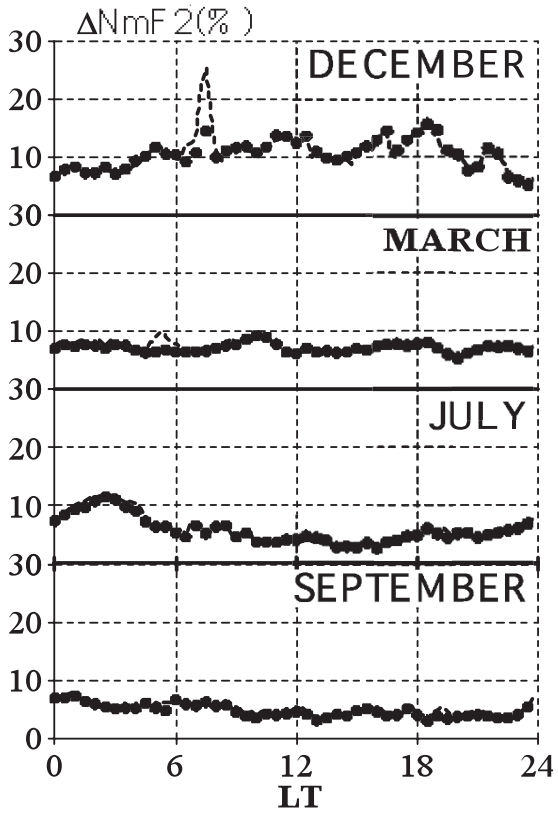

Fig. 1. Relative root mean square deviations ($\Delta N_m F_2$) between 15-minute time step medians of $N_m F_2$ and the values calculated with the LEMI under local steps equal to 0.5 hour (dashed line) and 1 hour (circles).

The model parameters P_0 (LT, M) and P_D (LT, M) can be obtained by the linear regression of P_{med} (LT, M, $F_{10.7}$) on $F_{10.7}$. The quality of the linear fit turns out to be dependent on the amount of averaging applied to the daily $F_{10.7}$ values. We tested different sliding window averaging periods for $F_{10.7}$ (from 27 days to 1 year) in order to minimize the linear regression RMS error. For most of the available P_{med} data, the 1 year period gave the best fit, with exception of December daytime, for which the 27 day period was optimal. Generally, median data are not well correlated with the solar activity intra year variations (from 27 days to 1 year) with the exception of December daytime. This fact is in agreement with our previous studies (Ratovsky *et al.*, 2009) where the difference between the observed f_oF_2 medians and IRI prediction was found to be poorly correlated with the $F_{10.7}$ intra year variations. Finally, we selected the 1-year running mean of daily $F_{10.7}$ as a solar activity proxy input for LEMI.

Once P_0 (LT, M) and P_D (LT, M) sets are available for discrete values of LT (15 minute increments) and M (0 to 11), the next step is to interpolate them over LT and M so that P_0 and P_D can be obtained for any given local time and month. We used a cardinal B-spline approximation (Schoenberg, 1969) to represent P_0 and P_D sets continuously, calculating the spline coefficients with a fixed month step $\Delta M = 1$ and various local time steps ΔLT ranging

Table 1. Construction of the LEMI model.

1. Calculation of the 27-day running medians of the ionospheric characteristics $P_{\rm med}$ (LT, D, Y).
2. Transformation of $P_{\rm med}$ (LT, D, Y) to $P_{\rm med}$ (LT, M, Y_S) at equal month steps using linear interpolation.
3. Calculation of the two sets of model parameters, (a) low solar activity set P_0(LT, M) and (b) slope of the linear dependence on $F_{10.7}$, $P_{\rm D}$ (LT, M), using the linear regression of $P_{\rm med}$ (LT, M, $F_{10.7}$) on 1-year running mean of $F_{10.7}$.
4. Calculation of the B-spline coefficients for P_0 and $P_{\rm D}$ sets with local time step ΔLT = 0.5 hour and month step ΔM = 1.

from 0.25 to 1 hour to select the optimal time resolution of the approximation. Figure 1 shows the relative root mean square differences $\Delta N_{\rm m}F_2$ between 15-minute time step medians of $N_{\rm m}F_2$ and the LEMI values with ΔLT resolution of 0.5 and 1.0 hour. The $\Delta N_{\rm m}F_2$ values are obtained by averaging the differences over all the years of observations for each month. Observed differences are due to the $F_{10.7}$ linear regression error and inaccuracy of the B-spline approximation. We found that $\Delta N_{\rm m}F_2$ values observed for different local time resolutions ΔLT are very similar except for the morning time interval around 7–8 LT in December. Such similarity is typical for all winter months, and for this reason we used 0.5-hour local time step for all B-spline approximations. Table 1 summaries the important steps required for the construction of the LEMI model.

In order to compare LEMI results with the IRI empirical model we calculated P_0 and $P_{\rm D}$ coefficients using IRI predicted values as the source data and following steps 2–4 of the technique. The comparisons are presented in following sections

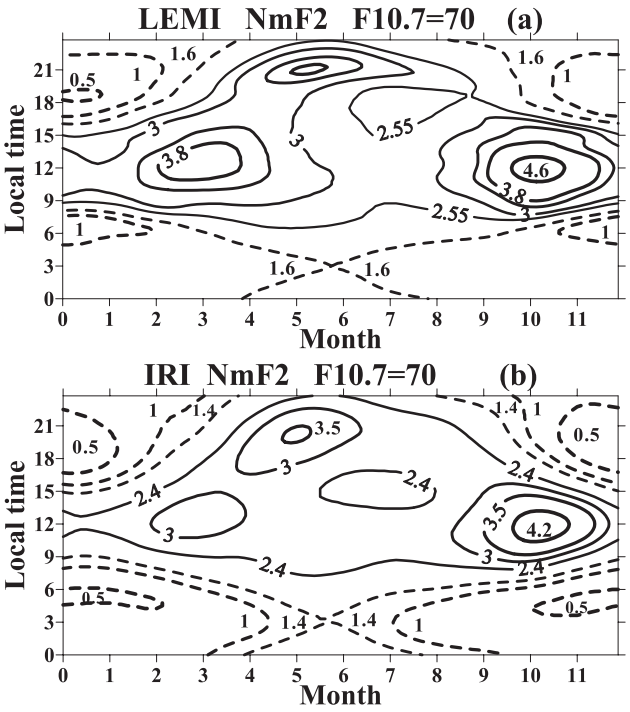

Fig. 2. Diurnal-seasonal variations of $N_{\rm m}F_2$ in [10^5 cm^{-3}] under low solar activity for LEMI (a) and IRI (b). The high and low values are depicted by the solid and dashed contours, respectively.

3. Results and Discussion

3.1 $N_{\rm m}F_2$ morphology

The LEMI diurnal-seasonal behavior of $N_{\rm m}F_2$ for low solar activity ($F_{10.7}$ = 70 s.f.u.) as a function of local time LT and month M is shown in Fig. 2(a). The high and low values are depicted by the solid and dashed contours, respectively. The daytime seasonal variations show two local maxima: in March ($\sim 4\cdot10^5$ cm^{-3}) and October ($\sim 5\cdot10^5$ cm^{-3}) and two local minima: in January ($\sim 3.1\cdot10^5$ cm^{-3}) and July ($\sim 2.7\cdot10^5$ cm^{-3}). The nighttime $N_{\rm m}F_2$ is largest in June and smallest in January, with intermediate values between these months. Maximum $N_{\rm m}F_2$ during the late evening hours (20–22 LT) occurs in May, one month earlier than during the nighttime.

The Irkutsk daytime seasonal pattern of $N_{\rm m}F_2$ differs from the Millstone Hill pattern (Lei *et al.*, 2005) where daytime $N_{\rm m}F_2$ is largest in the winter and smallest in the summer, with intermediate values at equinoxes. This difference has been reproduced by the Coupled Thermosphere-Ionosphere-Plasmasphere model (Zou *et al.*, 2000) and explained by the dependence of the winter down welling zone latitude on the geomagnetic longitude (Rishbeth *et al.*, 2000a) that makes a "far-from-the-pole" station (Irkutsk) different from a "near-the-pole" station (Millstone Hill) during the same season.

We can distinguish three types of $N_{\rm m}F_2$ diurnal behavior under low solar activity. The winter-like (October–February) pattern is characterized by the main maximum near noon, the local post midnight maximum (2–2:30 LT), and two local minima in the evening (18:30–21 LT) and in the morning (6–7 LT). Typical summer (May–July) behavior is characterized by the main evening maximum ($\sim$21 LT), the main morning minimum ($\sim$3 LT), the local prenoon maximum ($\sim$11 LT), and the local afternoon minimum (15 LT in May and 17 LT in June, July). Typical equinox (March, September) pattern is characterized by only one maximum near noon and one minimum in the morning ($\sim$5 LT).

The IRI prediction (Fig. 2(b)) of the $N_{\rm m}F_2$ diurnal-seasonal behavior under low solar activity reproduces the LEMI pattern reasonably well, though IRI systematically underestimates both the maxima and minima of $N_{\rm m}F_2$ obtained with LEMI.

The study of the $P_{\rm D}$ slope as a function of LT and M provides insight into how the ionospheric diurnal-seasonal pattern changes with increasing solar activity. Figure 3(a) shows the LEMI diurnal-seasonal behavior of the $N_{\rm m}F_{2\rm D}$ in [10^5 cm^{-3}/100 s.f.u.] units. The daytime $N_{\rm m}F_2$ (11–13 LT) is most sensitive to solar activity near the winter solstice ($N_{\rm m}F_{2\rm D} \sim$ 14 10^5 cm^{-3}/100 s.f.u.) and least sensitive near the summer solstice ($N_{\rm m}F_{2\rm D}$ $\sim$3–3.6 10^5 cm^{-3}/100 s.f.u.), with intermediate values at equinoxes (9–10.5 10^5 cm^{-3}/100 s.f.u. in March and 7–8.5 10^5 cm^{-3}/100 s.f.u. in

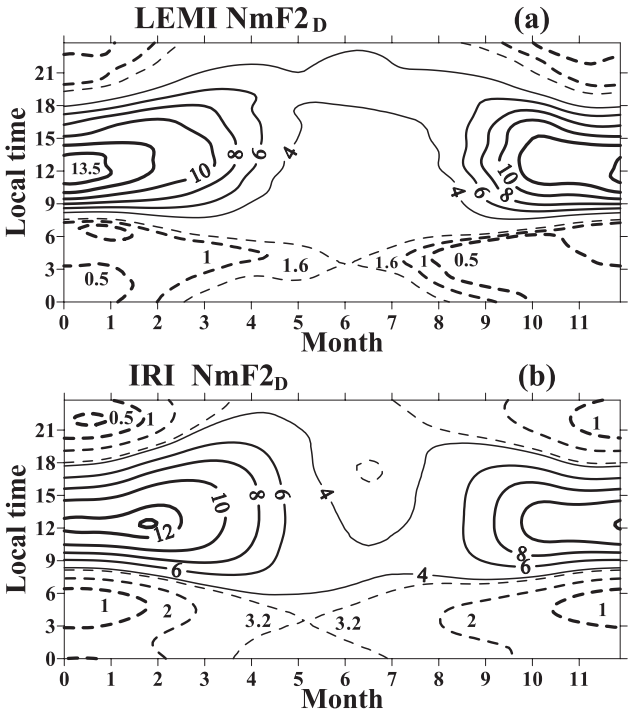

Fig. 3. Diurnal-seasonal variations of the slope of the linear dependence on $F_{10.7}$, N_mF_{2D} in [10^5 cm^{-3}/100s.f.u.] for LEMI (a) and IRI (b). The high and low values are depicted by the solid and dashed contours, respectively.

September). Thus, with increasing solar activity the daytime N_mF_2 peak moves from March and October towards the winter solstice. This peculiar behavior agrees with the ionospheric maps developed by Torr and Torr (1973) that, for high solar activity, reproduce larger values of winter critical frequency f_oF_2 than the summer and equinox f_oF_2 for all considered midlatitude stations. The Irkutsk LEMI daytime seasonal pattern of the N_mF_{2D} agrees with both Millstone Hill (Lei *et al.*, 2005) and the IRI patterns (Fig. 3(b)).

According to LEMI (Fig. 3(a)), the summer (May–July) diurnal behavior of N_mF_2 is characterized by the highest sensitivity to solar activity during the evening hours ($N_mF_{2D} \sim$ 19–20 LT, 4–5 10^5 cm^{-3}/100 s.f.u.), the lowest sensitivity during the morning ($N_mF_{2D} \sim$ 3:30 LT, $\sim$1.5 10^5 cm^{-3}/100 s.f.u.), and monotonic increase from morning to evening. Such LEMI behavior means that the prenoon N_mF_2 maximum that we observed in the summer diurnal pattern for low $F_{10.7}$ disappears with increasing solar activity. As for the IRI prediction (Fig. 3(b)), the diurnal maximum of the summer N_mF_{2D} is seen at prenoon and noon hours, rather than in the evening, which makes the evening and prenoon maxima of N_mF_2 comparable to each other with increasing solar activity. This disagreement between the IRI-predicted and the observed summer diurnal behavior of f_oF_2 was discussed previously by Ratovsky *et al.* (2009). The Irkutsk summer diurnal behavior of the N_mF_{2D} slope differs from the Millstone Hill behavior (Lei *et al.*, 2005), where the summer N_mF_{2D} varies only weakly during the day (2–3 10^5 cm^{-3}/100 s.f.u.).

Figure 3(a) also demonstrates that there is an area of extremely weak dependence of N_mF_2 on solar activity ($N_mF_{2D} < 0.5\ 10^5$ cm^{-3}/100 s.f.u.) in the postmidnight hours. This means that the enhancement of postmidnight N_mF_2 gets weaker with increasing solar activity, which agrees with the studies of Mikhailov *et al.* (2000). The authors explained this phenomenon by suggesting that the nighttime recombination rate increases faster than the nighttime influx from the plasmasphere with increasing solar activity.

Ratovsky *et al.* (2009) observed that the solar activity dependence of the diurnal f_oF_2 minimum at Irkutsk is much weaker than the IRI prediction. This disagreement manifests itself in the difference between the postmidnight N_mF_{2D} obtained with LEMI and IRI. According to IRI, the average postmidnight (0–3 LT) N_mF_{2D} varies from 1.1 to 3.5 10^5 cm^{-3}/100 s.f.u. (from December to June), whereas the LEMI values are 0.4 and 2.5 10^5 cm^{-3}/100 s.f.u. for December and June, respectively. The Millstone Hill (Lei *et al.*, 2005) average postmidnight summer N_mF_{2D} is close to the LEMI value, whereas the winter N_mF_{2D} is close to the IRI prediction for Irkutsk. Possibly, the balance between the recombination rate and the plasmasphere influx, and hence the postmidnight N_mF_{2D} depends on the geographic location. In support of this explanation, modeling by Zou *et al.* (2000) showed that the December midnight ratio N_mF_2 ($F_{10.7} = 180$)/N_mF_2 ($F_{10.7} = 100$) is the smallest at "far-from-the-pole" longitudes.

3.2 h_mF_2 morphology

Figure 4(a) shows the LEMI diurnal-seasonal behavior of the F_2 peak height h_mF_2 under low solar activity ($F_{10.7} = 70$ s.f.u.). The high (nighttime) and low (daytime) values are depicted by the solid and dashed contours, respectively. The average daytime (10–14 LT) seasonal variations show an annual pattern with the December minimum (209 km) and the April–May maximum (228 km). The average nighttime (22–02 LT) seasonal variations also show an annual pattern with the June–July minimum (282 km) and the November maximum (294 km). Both daytime and nighttime seasonal patterns of LEMI are somewhat different from the IRI model (Fig. 4(b)) that predicts a semiannual pattern both for average daytime (10–14 LT) and nighttime (22–02 LT) h_mF_2. The daytime h_mF_2 has local maxima in March (243 km) and September (240 km), and local minima in July (210 km) and January (218 km). The nighttime h_mF_2 has local maxima in March (324 km) and October (313 km), and local minima in July (292 km) and December (302 km).

Figure 5(a) shows diurnal-seasonal dependence of h_mF_2 on solar activity by plotting h_mF_{2D} values in units of [km/100 s.f.u.]. The peak height of the ionosphere is most sensitive to the solar activity ($h_mF_{2D} > 70$) in the postmidnight hours. Another area of strong dependence ($h_mF_{2D} >$ 60) is seen in the afternoon hours in October and from March to August. The area of weak dependence of h_mF_2 on solar activity ($h_mF_{2D} < 50$) is seen in the prenoon hours for all months except October and in the late evening hours for all months except June and July.

The pattern of the LEMI diurnal-seasonal behavior of h_mF_{2D} is different from both the IRI prediction (Fig. 5(b)) and the Millstone Hill data (Lei *et al.*, 2005). IRI predicts that the h_mF_{2D} is approximately proportional to the

Table 2. Daytime and nighttime annual mean of h_mF_2 ($F_{10.7} = 140$) in [km] and h_mF_{2D} in [km/100 s.f.u.] for different stations. The station coordinates are shown in parentheses. Dip is the magnetic field dip angle of the station.

Station	Dip (°)	Daytime		Nighttime	
		h_mF_2 ($F_{10.7} = 140$)	h_mF_{2D}	h_mF_2 ($F_{10.7} = 140$)	h_mF_{2D}
Sodankyla (67N, 27E)	76	270	35	374	46
Moscow (56N, 37E)	71	268	46	374	50
Irkutsk (52N, 104E)	**72**	**263**	**61**	**340**	**73**
IRI prediction for Irkutsk		272	66	331	36
Slough (52N, 1W)	67	258	48	378	43
Millstone Hill (43N, 288E)	70	265	46	333	33
Wallops Is (38N, 75W)	70	268	44	348	37
Wakkanai (38N, 142E)	**51**	**272**	**57**	**366**	**56**
Norfolk Is (29S, 168E)	56	282	45	340	38
Mundaring (32S, 116E)	66	275	38	338	33
Kerguelen (49S, 70E)	67	297	40	340	48
Port Stanley (52S, 58W)	**47**	**261**	**61**	**387**	**55**

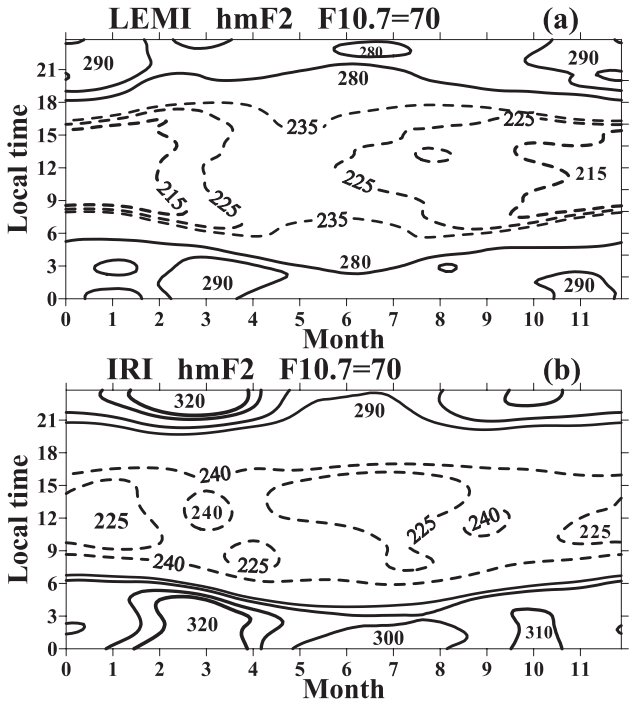

Fig. 4. Diurnal-seasonal variations of h_mF_2 in [km] under low solar activity for LEMI (a) and IRI (b). The high and low values are depicted by the solid and dashed contours, respectively.

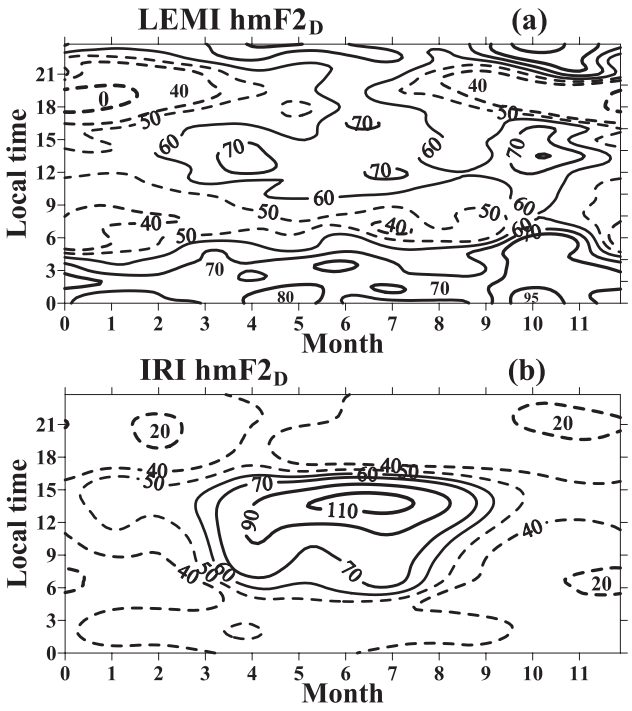

Fig. 5. Diurnal-seasonal variations of the slope of the linear dependence on $F_{10.7}$, h_mF_{2D} in [km/100 s.f.u.] for LEMI (a) and IRI (b). The high and low values are depicted by the solid and dashed contours, respectively.

solar zenith angle, so that highest sensitivity to increasing solar activity level ($h_mF_{2D} > 60$) is seen in the daytime hours (~6–15 LT) for the summer and equinox months. At Millstone Hill (Lei *et al.*, 2005) h_mF_{2D} remains below 56 km/100 s.f.u., with higher values during daytime than at night, a diurnal peak at around 1300–1400 LT in all seasons, and a weaker dependence in winter than in other seasons.

We compared the LEMI daytime (10–14 LT) and nighttime (22–02 LT) annual mean of h_mF_{2D} with values observed at midlatitude stations (Rishbeth *et al.*, 2000b). Table 1 demonstrates the daytime and nighttime annual mean of h_mF_{2D} and h_mF_2 ($F_{10.7} = 140$ s.f.u.). Except for Irkutsk and Millstone Hill, the observational data are taken from the paper of Rishbeth *et al.* (2000b). The Irkutsk h_mF_2 ($F_{10.7} = 140$) was calculated using expression (1) and LEMI values of h_mF_{20} and h_mF_{2D}. Using the same technique, we calculated Millstone Hill h_mF_2 ($F_{10.7} = 140$) using the data of Lei *et al.* (2005). One can see from Table 2 that h_mF_2 is most sensitive to solar activity for the "far-from-the-pole" stations (Port Stanley, Wakkanai, Irkutsk) and this sensitivity is not correlated to the magnetic field dip angle.

3.3 B_0 morphology

The LEMI diurnal-seasonal behavior of the bottomside thickness B_0 under low solar activity ($F_{10.7} = 70$ s.f.u.) is shown in Fig. 6(a). The high and low values are depicted by the solid and dashed contours, respectively.

Table 3. Mean nighttime (22–02 LT) and mean daytime (10–14 LT) values of B_{0D} in [km/100 s.f.u.] averaged over the three seasons.

Season	Nighttime			Daytime		
	Irkutsk LEMI	IRI prediction for Irkutsk	Millstone Hill	Irkutsk LEMI	IRI prediction for Irkutsk	Millstone Hill
Winter	18	11	15	15	14	15
Equinox	19	12	15	19	22	15
Summer	28	12	30	20	48	20

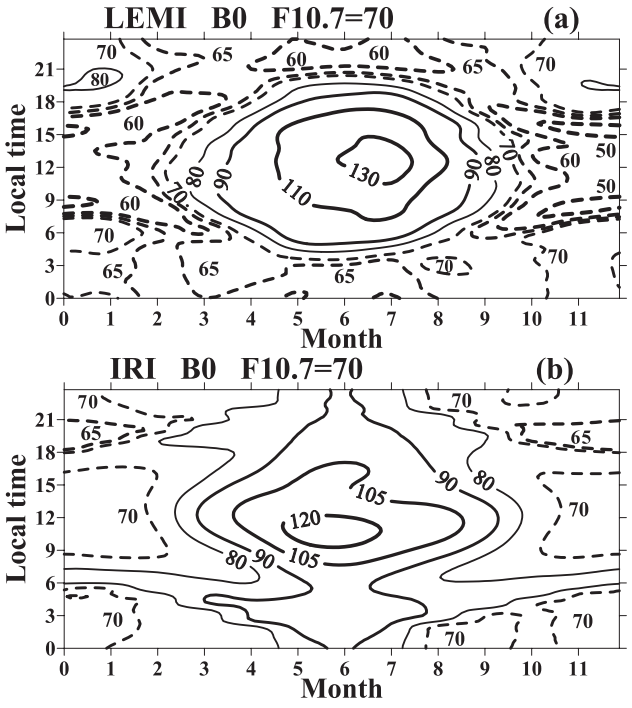

Fig. 6. Diurnal-seasonal variations of B_0 in [km] under low solar activity for LEMI (a) and IRI (b). The high and low values are depicted by the solid and dashed contours, respectively.

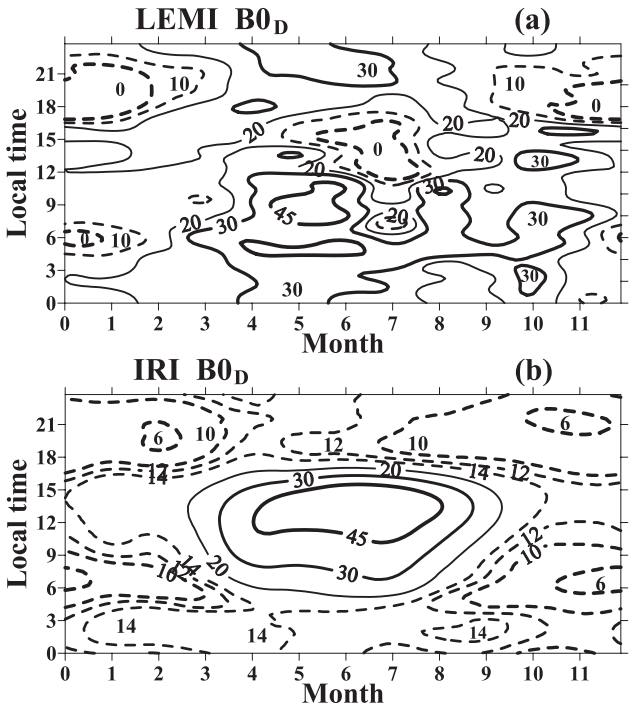

Fig. 7. Diurnal-seasonal variations of the slope of the linear dependence on $F_{10.7}$, B_{0D} in [km/100 s.f.u.] for LEMI (a) and IRI (b). The high and low values are depicted by the solid and dashed contours, respectively.

Diurnal behavior of B_0 during winter and equinox (from September to March) is characterized by so called morning and evening collapses (Lei *et al*., 2004) when B_0 is minimal. The local times of the collapses (8:45–6:00 and 15:15–18:00 LT) are close to the times of sunrise and sunset at zero altitude. The B_0 at the minima increases from 47–48 km at the winter solstice to 57–63 km at the spring and autumn equinoxes. In November–January the midnight B_0 (70–75 km) exceeds the noon one (56–59 km), in March and September the noon B_0 (84 km) exceeds the midnight one (66–69 km), and in October and February the noon and midnight B_0 values (64–68 km) are comparable. So, in winter and equinox months the diurnal-seasonal pattern of B_0 is close to being symmetric about noon as well as the winter solstice. The summer-like (April–August) diurnal behavior is characterized by the only one maximum near noon (12:30–12:45 LT) and one minimum in the late evening hours (21:15–21:45 LT, $B_0 = \sim$60 km). Maximum diurnal B_0 values rise from 99 km in April to 137 km in July and after that decrease to 116 km in August. The average daytime (10–14 LT) seasonal variations of B_0 show an annual pattern with the December minimum (56 km) and the July maximum (133 km). The average nighttime (22–02 LT) seasonal variations also show an annual pattern with the May minimum (63 km) and the November maximum (75 km).

In general, diurnal-seasonal pattern of B_0 is close to that at Millstone Hill (Lei *et al*., 2004). There are differences in the nighttime behavior. At Millstone Hill the winter noon and midnight values are close together, and the nighttime B_0 does not show an evident seasonal effect.

The LEMI diurnal-seasonal behavior of B_0 is somewhat different from the IRI prediction (Fig. 6(b)). IRI predicts a well-pronounced morning maximum (dominant for the winter months), which is not observed in the LEMI pattern. The IRI's evening collapse occurs later in the evening hours (18–21 LT) in comparison to LEMI. Both models give comparable daytime seasonal patterns of B_0, though IRI overestimates the winter B_0 and underestimates the summer B_0. Compared to LEMI, the IRI predicts an opposite nighttime seasonal behavior with the December minimum (68 km) and the June maximum (92 km).

The LEMI diurnal-seasonal behavior of the B_0 sensitivity to increasing solar activity level, B_{0D}, is shown in Fig. 7(a). No clear diurnal-seasonal pattern of B_{0D} can be seen. In contrast to LEMI, IRI gives a clear pattern of B_{0D}

(Fig. 7(b)). Similar to $h_{\mathrm{m}}\mathrm{D}$ IRI preducts greater dependence of B_0 on solar activity ($B_{0\mathrm{D}} > 60$ km/100 s.f.u.) in the daytime hours (~6–15 LT) from March to September.

Millstone Hill data (Lei *et al*., 2004) suggest that increase of solar activity level from low ($F_{10.7} = 90$ s.f.u.) to high ($F_{10.7} = 180$ s.f.u.) results in increase of B_0 by about 30% during the night and by about 20% during the day, except for the morning collapse periods in equinox and winter when B_0 increases by less than 10%. In order to compare these observations with LEMI, we had to regroup and average our data to match Lei *et al*. (2004) technique of binning data into three seasons, namely summer (May–August), winter (November–February), and equinox (March, April, September and October). We averaged the LEMI and IRI mean nighttime (22–02 LT) and mean daytime (10–14 LT) values of $B_{0\mathrm{D}}$ over the three seasons. Using available Millstone Hill observations of B_0 under low ($F_{107} = 90$ s.f.u.) and high ($F_{107} = 180$ s.f.u.) solar activity (Lei *et al*., 2004), we obtained estimates of $B_{0\mathrm{D}}$. Table 3 shows the final results. For the nighttime, the IRI $B_{0\mathrm{D}}$ does not show any seasonal variations; whereas both the Irkutsk LEMI and Millstone Hill summer $B_{0\mathrm{D}}$ noticeably exceeds the winter one and the equinox $B_{0\mathrm{D}}$ is close to the winter one. In all presented cases, the summer daytime $B_{0\mathrm{D}}$ exceeds the winter one, but the IRI summer daytime $B_{0\mathrm{D}}$ noticeably overestimates both the Irkutsk LEMI and Millstone Hill ones.

4. Conclusion

Data from routine ionospheric observations at Irkutsk, Russia using a DPS-4 Digisonde sounder were used to derive a local empirical model of the electron density that provides a comprehensive description of the diurnal, seasonal, and solar activity variations of the major ionospheric characteristics. We have compared the local model patterns with the IRI-2007 prediction (Bilitza and Reinisch, 2008) and the retrospective data from long-term mid-latitude measurements by the Millstone Hill incoherent scatter radar and the collocated Digisonde (Lei *et al*., 2004, 2005).

The comparison revealed both similarities and differences between Irkutsk and Millstone Hill diurnal, seasonal and solar activity variations. The observed disagreements can in part be explained by the different location of the instruments at "far-from-the-pole" and "near-the-pole" longitudes. The observed strong dependence of the nighttime $h_{\mathrm{m}}F_2$ on the level of solar activity is found to be in agreement with the observations at "far-from-the-pole" sites reported by Rishbeth *et al*. (2000b). Many of the local Irkutsk model features, such as the diurnal-seasonal pattern of $N_{\mathrm{m}}F_2$ under low solar activity and the slope of the daytime $N_{\mathrm{m}}F_2$ dependence on $F_{10.7}$, are reasonably well reproduced by the IRI prediction, although there are differences.

In winter and equinox months the diurnal-seasonal pattern of B_0 under low solar activity is found to be nearly symmetric about noon as well as the winter solstice. This feature will be useful for empirical modeling. The local model does not give a clear diurnal-seasonal pattern of the slope of B_0 dependence on $F_{10.7}$, but season averages of the daytime and nighttime B_0 do agree with available Millstone Hill observations.

Acknowledgments. The authors would like to thank Dr. Ivan Galkin of UMass Lowell Center for Atmospheric Research for his helpful comments and suggestions.

References

Bilitza, D. and B. Reinisch, International Reference Ionosphere 2007: Improvements and new parameters, *J. Adv. Space Res*., **42**, 599–609, 2008.

Brynko, I. G., I. A. Galkin, V. P. Grozov, N. I. Dvinskikh, S. M. Matyuoshonok, and V. E. Nosov, An automatically controlled data gathering and processing system using an FMCW ionosonde, *Adv. Space Res*., **8**, 121–124, 1988.

Lei, J., L. Liu, W. Wan, S.-R. Zhang, and J. M. Holt, A statistical study of ionospheric profile parameters derived from Millstone Hill incoherent scatter radar measurements, *Geophys. Res. Lett*., **31**, L14804, doi:10.1029/2004GL020578, 2004.

Lei, J., L. Liu, W. Wan, and S.-R. Zhang, Variations of electron density based on long-term incoherent scatter radar and ionosonde measurements over Millstone Hill, *Radio Sci*., **40**, RS2008, doi:10.1029/2004RS003106, 2005.

Khmyrov, G. M., I. A. Galkin, A. V. Kozlov, B. W. Reinisch, J. McElroy, and C. Dozois, Exploring digisonde ionogram data with SAO-X and DIDBase, *Radio Sounding and Plasma Physics*, *AIP Conf. Proc*., **974**, 175–185, 2008.

Mikhailov, A. V., M. Förster, and T. Y. Leschinskaya, On the mechanism of the post-midnight winter NmF2 enhancements: dependence on solar activity, *Ann. Geophys*., **18**, 1422–1434, 2000.

Ratovsky, K. G., V. P. Grozov, A. G. Kim, A. V. Medvedev, A. P. Potekhin, and B. G. Shpynev, Comparison of the ionospheric F Region parameters measured with the DPS-4 Digisonde, LFM ionosonde, and incoherent backscatter radar in Irkutsk during the magnetic storm of October 29–31, 2003, *Geomagn. Aeron*., **45**, 129–133, 2005.

Ratovsky, K. G., A. V. Oinats, and A. V. Medvedev, Diurnal and seasonal variations of F2 layer characteristics over Irkutsk during the decrease in solar activity in 2003–2006: Observations and IRI-2001 model predictions, *Adv. Space Res*., **43**, 1806–1811, 2009.

Reinisch, B. W. and X. Huang, Automatic calculation of electron density profiles from digital ionograms, 3, Processing of bottomside ionograms, *Radio Sci*., **18**, 477–492, 1983.

Reinisch, B. W. and X. Huang, Finding better B0 and B1 parameters for the IRI F2-profile function, *Adv. Space Res*., **22**, 741–747, 1998.

Reinisch, B. W., D. M. Haines, K. Bibl, I. Galkin, X. Huang, D. F. Kitrosser, G. S. Sales, and J. L. Scali, Ionospheric sounding support of OTH radar, *Radio Sci*., **32**, 1681–1694, 1997.

Reinisch, B. W., I. A. Galkin, G. Khmyrov, A. Kozlov, and D. F. Kitrosser, Automated collection and dissemination of ionospheric data from the digisonde network, *Adv. Radio Sci*., **2**, 241–247, 2004.

Rishbeth, H., I. C. F. Müller-Wodarg, L. Zou, T. J. Fuller-Rowell, G. H. Millward, R. J. Moffett, D. W. Idenden, and A. D. Aylward, Annual and semiannual variations in the ionospheric F2-layer: II. Physical discussion, *Ann. Geophys*., **18**, 945–956, 2000a.

Rishbeth, H., K. J. F. Sedgemore-Schulthess, and T. Ulich, Semiannual and annual variations in the height of the ionospheric F2-peak, *Ann. Geophys*., **18**, 285–299, 2000b.

Schoenberg, I. J., Cardinal interpolation and spline functions, *J. Approximation Theory*, **2**, 167–206, 1969.

Shpynev, B. G., Incoherent scatter Faraday rotation measurements on a radar with single linear polarization, *Radio Sci*., **39**, RS3001, doi:10.1029/2001RS002523, 2004.

Torr, M. R. and D. G. Torr, The seasonal behaviour of the F2-layer of the ionosphere, *J. Atmos. Terr. Phys*., **35**, 2237–2251, 1973.

Zou, L., H. Rishbeth, I. C. F. Müller-Wodarg, A. D. Aylward, G. H. Millward, T. J. Fuller-Rowell, D. W. Idenden, and R. J. Moffett, Annual and semiannual variations in the ionospheric F2-layer: I. Modelling, *Ann. Geophys*., **18**, 927–944, 2000.

K. G. Ratovsky (e-mail: ratovsky@iszf.irk.ru) and A. V. Oinats